Noname manuscript No.
(will be inserted by the editor)

Growth Patterns of Abdominal Atherosclerotic Calcified Deposits from Lumbar Lateral X-rays

Lene Lillemark · Melanie Ganz · Natasha Barascuk · Erik B. Dam · Mads Nielsen

Received: date / Accepted: date

Abstract The aim of this study is to investigate new methods for describing the progression of atherosclerosis based on novel information of the growth patterns of individual abdominal aortic calcifications (AACs) over time. Lateral X-ray images were used due to their low cost, fast examination time, and wide-spread use, which facilitates a large statistical model (n $>$ 100) based on longitudinal data. The examined cohort consisted of 103 post-menopausal women aged 62.4 y ($\pm$ 7.0 y) with an average number of AACs of 4.7 ($\pm$ 8.0) at baseline. The subjects had X-ray images taken in 1992-93 (baseline) and again in 2000-01 (follow-up). The growth patterns of the individual AACs were derived based on registered baseline and follow-up images. Area, height, width, centre of mass position, and movement of the centre of mass, and upper and lower boundary of the matched AACs were measured. The AACs occurred first, mainly, on the posterior aortic wall. The AACs grew on average 41 % in the longitudinal direction and 21 % in the radial direction. A correlation of 0.48 ($P < 0.001$) between growth in width and height of the AACs was present. The centre of mass of the AACs moved 0.60 mm ($P < 0.001$) downstream in the aorta, on average. The growth patterns of AACs may give new insights into the progression of atherosclerosis. The downstream asymmetry in the growth patterns indicates variability in microscopic environments around the AACs.

Department for Computer Science, University of Copenhagen
Universitetsparken 1, 2100 Copenhagen Ø, Denmark
Tel.: +45-35 32 14 00
Fax: +45-35 32 14 01
E-mail: lene@diku.dk

Nordic Bioscience Imaging
Herlev Hovedgade 207, 2730 Herlev, Denmark

Keywords Atherosclerosis · Abdominal Aortic Calcification · Growth patterns · X-ray

1 Introduction

Atherosclerosis is usually the underlying pathology of cardiovascular diseases (CVD) [1], and CVD are the leading cause of death in Europe and the United States [2,3]. It has been demonstrated that abdominal aortic calcifications detected by lateral lumbar radiographs are markers of subclinical atherosclerotic disease and an independent predictor of subsequent vascular morbidity and mortality [1,4,5]. We are interested in studying vascular calcifications because these provide important prospective information when assessing the risk of CVD [1]. Thus, the vascular calcifications in atherosclerosis play an important role in acute CVD events like myocardial infarction, strokes, and sudden death [6,7].

Imaging modalities such as intravascular ultrasound (IVUS), computed tomography (CT), and magnetic resonance imaging (MRI) have previously been used for studies of the progression of atherosclerosis [8–11]. It can be problematic to use these image modalities for large scale clinical studies and screening programs. The problems are the invasiveness and the ring-down artifacts produced by acoustic oscillations in the case of IVUS, the high cost and the slow patient throughput for MRI images, and the unclarified relationship between cancer and the radiation in CT imaging [12,8, 13,14].

X-ray imaging is an attractive imaging modality for quantification of AACs because it has a low cost, fast examination time, and exposes subjects to a relative low radiation dose. Another advantage of X-ray images is that historical data already exist from many clin-

ical trials and routine screenings for osteoporosis [15], which can be used in risk assessment based on the identification of the growth patterns of AACs. This study is based on X-rays images due to the historical X-ray data we have access to, but alternatively ultrasound (US) imaging could be used for identification of the growth patterns. US produces no ionising radiation and is therefore suitable for use in evaluation and monitoring of carotid atherosclerosis in large scale longitudinal studies and in clinical management of patients at risk of stroke [16–18]. US is also used, routinely, for vascular assessment and screening for abdominal aortic aneurysms [19–21].

Our hypothesis is that growth patterns may provide useful estimators of the progression of atherosclerosis. The gold standard severity score for atherosclerotic calcifications is the AC24 score, introduced by the Framingham group [22,23]. It is a quantitative scoring system for measuring the extent of calcified tissue along the arterial wall. To our knowledge, this is the first study that characterises the growth patterns of individual AACs based on X-ray images. The aim is to evaluate the growth patterns of the calcified deposits in order to gain more information about the progression of atherosclerosis.

2 Materials and methods

2.1 Study population

The study population was taken from a previously published longitudinal study on metabolic risk factors in relation to CVD and osteoporosis, starting in 1992-93 (baseline), when 686 postmenopausal women participated [15]. The follow-up visit was performed in 2000-01. The subjects were recruited via questionnaires, and the study was approved according to the Helsinki Declaration II and the European Standards to Good Clinical Practice. All subjects gave their written consent. The study population is illustrated in Figure 1. From the original study population, 256 subjects had a visible lumbar aorta in a single radiograph at both baseline and follow-up. 103 of these subjects had AACs at both baseline and follow-up visit. Numerous traditional risk parameters were collected for the study participants including age, height, smoking, body mass index (BMI), waist and hip circumference, systolic and diastolic blood pressure, treated hypertension, daily alcohol and coffee intake, and weekly fitness activity. Biochemical measurements of fasting glucose, a lipid profile including total cholesterol, triglycerides, LDL-cholesterol, HDL-cholesterol, and apolipoproteins were obtained from blood samples at baseline and follow-up. The average age of our subjects was 62.4 y (± 7.0 y) and the average BMI was 24.1 kg/m^2 (± 4.0 kg/m^2) at the initial scanning, as shown in Table 1.

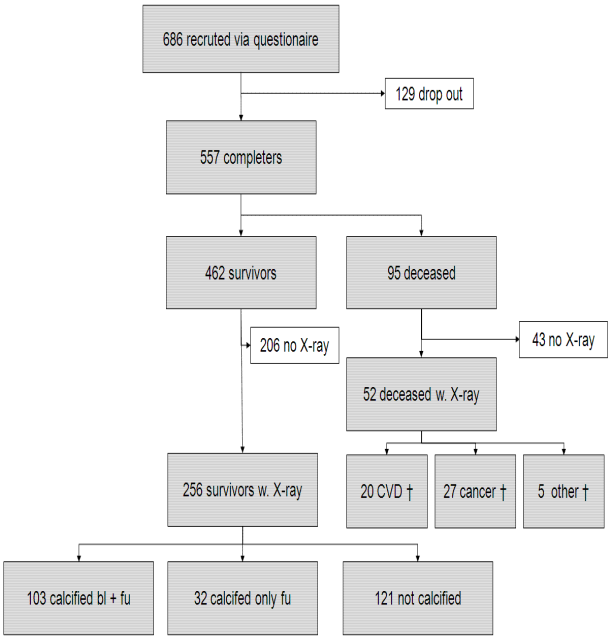

Fig. 1 The subject selection, which resulted in 103 subjects who had calcified plaque at both baseline and follow-up. bl stands for baseline, and fu stands for follow-up.

Table 1 Subjects participating in the study of growth patterns. Mean values and standard deviations for baseline and follow-up.

	Baseline	Follow-up
Age (years)	62.4 (±7.0)	70.9 (±7.0)
BMI range (kg/m^2)	24.1 (±4.0)	24.9 (±4.5)
Diastolic BP (mmHg)	83.4 (±62.8)	83.6 (±11.9)
Systolic BP (mmHg)	131.2 (±21.0)	158.5 (±28.2)
Cholesterol (mmol/l)	6.66 (±1.26)	6.14 (±1.15)
Triglyceride (mmol/l)	1.23 (±0.55)	1.42 (±0.68)
Glucose (mmol/l)	5.50 (±1.41)	5.71 (±1.33)
LDL cholesterol (mmol/l)	3.09 (±0.89)	2.90 (±0.88)
HDL cholesterol (mmol/l)	1.77 (±0.45)	1.66 (±0.44)

2.2 Scanning and digital annotation

The images, used in the study, were lateral X-ray projections, which were digitalised with a Vidar DosimetryPro Advantage scanner with a pixel size of 44.6 μm × 44.6 μm. The images were scanned at the Centre for Clinical and Basic Research (CCBR) in Ballerup, Denmark. The images were annotated by three trained radiologists from CCBR that were blinded from time point

and morbidity. The annotations included the standard six points morphometric for each vertebra L1-L4 and a variable number of points on the posterior and anterior aorta wall and on the contours of the calcified deposits. From the data set, 103 subjects had baseline AACs with an average of 4.7 (± 8.0) AACs.

2.3 Quantification and characterisation

The images were scanned at two different time instances, resulting in changes in the body sizes, the subject's position in the X-ray scanner, calibrations of the scanner, and ageing in the anatomy of the subjects. This caused a significant variability in the position and the projective shape of the vertebrae, the aortas, and the AACs. The variability was compensated by registration where the aortas from the follow-up images were aligned with to the aortas on the baseline images. The registration was done from follow-up to baseline in order to get predictive growth patterns.

2.3.1 Image registration and matching

The follow-up images were registered to the baseline images with thin plate splines (TPS) registration [24]. TPS were chosen due to their ability for aligning the deformable aortas globally from a few landmarks. Landmarks on the intersections between the anterior and posterior aorta walls and the inter vertebrae lines were used for the registration, as illustrated in Figure 2. The Hausdorff distance between the baseline and the registered follow-up posterior and anterior aorta walls was measured to get an estimate of the registration precision. The growth of each AAC was measured based on individually matched AACs where area overlap (AO) was the used matching criterion. AO captures the corresponding AACs without assumptions of a certain shape or growth descriptor. Only one-to-one correspondent matches between the AACs were used to derive the growth patterns. An example of the matched AACs is shown in Figure 3.

2.3.2 Growth pattern analysis

The growth patterns of the matched AACs can be observed in three locally anatomically meaningful directions, which are the longitudinal (in the blood flow direction), the circumferential (around the aorta) and the radial (the direction into the aorta) direction.

The longitudinal growth would give an indication of whether the AACs occupy a longer part of the aorta wall, and it was measured as the change in height of the AACs. The radial growth was measured as the change in width of the AACs. The area of the AACs could give information about the overall growth of the AACs. The area combines contributions from the circumferential and radial directions due to the two dimensional projection of the three dimensional data. The projections may interfere the different directions, but the dense tissue of the AACs on the anterior/posterior sides of the aorta wall are well captured by the X-ray attenuation. The AACs in the middle part of the aorta are harder to distinguish from background tissue resulting in that the main part of the AACs in our study were aligned with the anterior or posterior aorta wall. The area of the AACs was based mainly on the radial and longitudinal direction. The longitudinal growth direction of the AACs was calculated as the movement of the center of masses of the corresponding AACs. To strengthen the longitudinal growth direction also movement of the upper and lower boundary of the AACs were measured. The movement of the center of mass was also used to give an indication of whether the calcifications grew into the center of the aorta or into the aorta wall. Figure 3 illustrates the measurements of the growth patterns.

An idealised aorta coordinate system was made to capture the growth patterns, in the three previous described directions, along the curvature of the aorta. The idealised aorta coordinates system was based on a vertical aorta in a coordinate frame with the same range as the original aortas, as illustrated in Figure 4. The idealised coordinate system made us able to base the growth analysis on known and uniform directions and coordinates for all images. Both baseline and follow-up images were registered to the idealised aorta coordinate system by TPS. A local idealised coordinate system with origin in the centre of mass for each AAC and the axes in the direction of the blood flow and per-

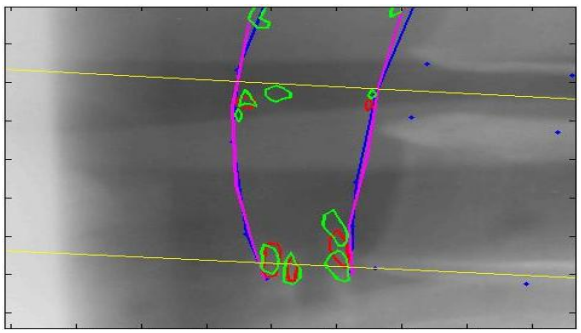

Fig. 2 The figure shows an example of the corresponding AACs. Blue represent the annotations of the baseline vertebrae and the baseline aorta walls, magenta represent the follow-up aorta registered to the baseline aorta, yellow represent the inter vertebrae lines, red represent the baseline AACs, and green the follow-up AACs. Note how area overlap was a good indicator of the matching AACs.

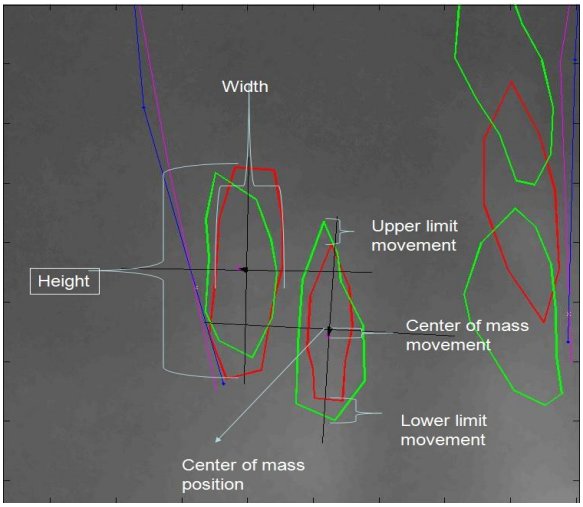

Fig. 3 The figure illustrates the growth patterns. Red represent the baseline AACs, green represent the follow-up AACs. The height, width, centre of mass position, and the movement in centre of mass, lower and upper boundary of the AACs are illustrated in the figure. The black lines correspond to the idealised coordinate system, from Figure 4(b), which reflects the curvature of the aorta. The paired AACs at the left are labeled one-to-one correspondent matches while the AACs at right are labeled as a one-to-many correspondent match, and they are therefore not included in the growth pattern analysis.

pendicular to the blood flow were formed based on the known directions from the idealised coordinate system, as shown in Figure 3.

The growth patterns were calculated based on the local idealised coordinate systems; the height of the AACs was measured along the "up"-direction and the width along the perpendicular axis. The area was measured as the total number of pixels inside the annotations of the AACs. The centre of mass (CM) of the AACs was measured as the position of the AAC in the aorta in the original image frame. We assumed the mass density as uniform. The changes in the CM position and the upper and lower boundary of the AACs were measured in the idealised local coordinate system for the baseline AACs. The total height of the vertebrae L1-L4 was also measured.

2.4 Statistical analysis

The growth patterns are expressed as signed means ± the standard deviation (SD) in the results. Differences were tested by a two sided heteroscedastic student's T-test, and the growth values were tested with a paired T-test both for which a P-value < 0.05 were considered to indicate statistical significance. Correlations between the growth factors were measured using the Pearson linear correlation coefficient with a 95 % confidence interval. All measurements were calculated per AAC independent of how many AACs each subject had.

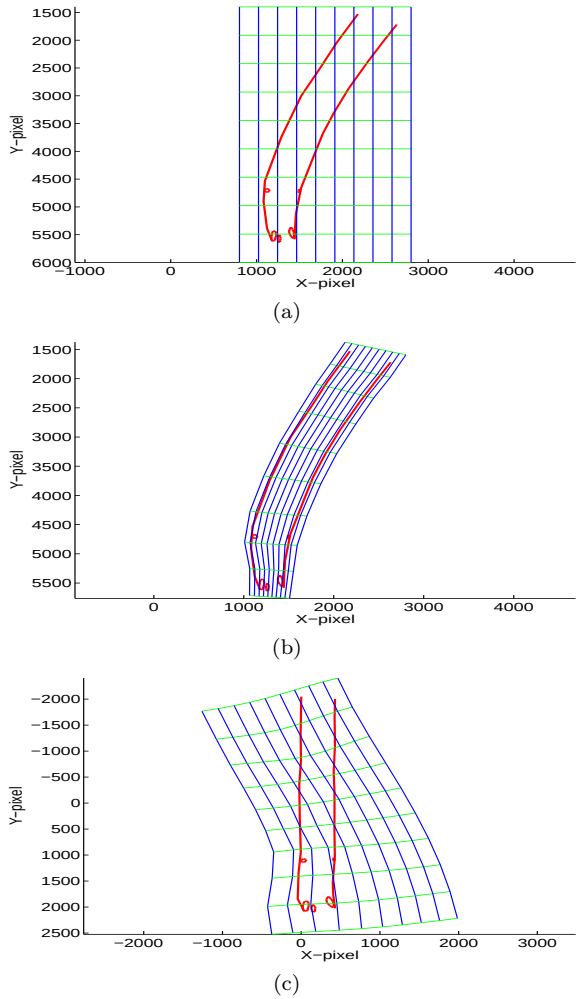

Fig. 4 4(a) shows an original image overlaid with a regular lattice. 4(b) shows an original aorta with the local idealised coordinate systems corresponding to the curvature of the aorta. 4(c) shows the idealised aorta with the overlaid corresponding lattice. The local idealised coordinate in 4(c) is derived based on this lattice.

3 Results

In Figure 5, the percentile number of subjects with less than or equal to the given number of AACs are shown. Also, the percentile number of AACs with less than or equal the given the area at both baseline and follow-up is shown in Figure 5. Figure 6 shows the distribution of the baseline and follow-up AACs, respectively.

The registration was validated based on the Hausdorff distance between the baseline aorta and the registered follow-up aorta. The average distances for the anterior and posterior aorta walls were 2.21 mm (± 1.82 mm) and 2.18 mm (± 1.94 mm), respectively.

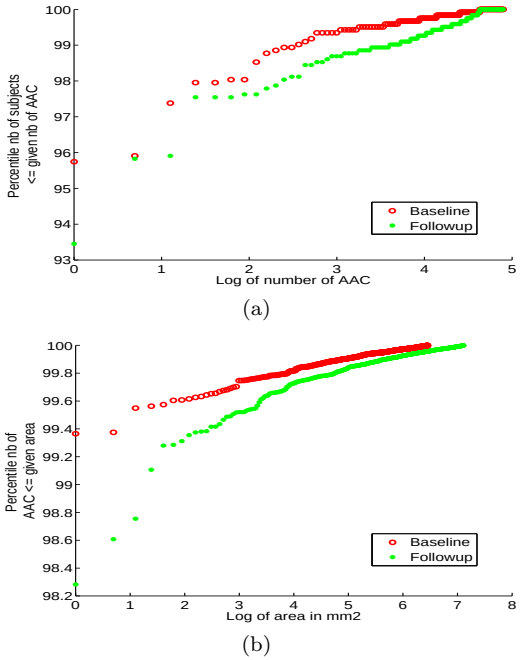

Fig. 5 5(a) shows the percentile number of subjects with less than or equal to the given number of AACs. 5(b) shows the percentile number of AACs with less than or equal to the given area of the AACs. The logarithm is used to get a visually clear separation between baseline and follow-up. The number of AACs increased during the study period, and the area of the existing AACs increased.

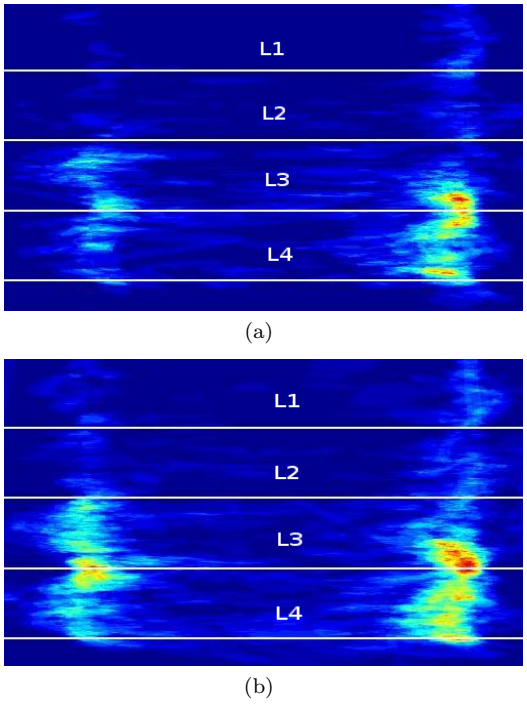

Fig. 6 6(a) shows a distribution map of the formation of all baseline AACs in the idealised image space. 6(b) shows a distribution map of the formation of all follow-up AACs. Note how the AACs mainly were placed on the posterior side of the aorta, and how new AACs appeared on the anterior aorta wall at follow-up.

Match rate was 38%. The total number of AACs at baseline was 633, and the number increased to 1222 at follow-up. The total match between baseline and follow-up one-to-one correspondent AACs was 38%. The growth patterns were calculated based on these matches. In 21% of the matches more than one baseline AAC matched to one follow-up AAC (the AACs may have grown together), and 9% of the baseline AACs were matched to more than one follow-up AAC. In 40% no correspondence between baseline and follow-up AACs were found, as shown in Table 2.

Table 2 The numbers for matches rounded to nearest decimal. The total match between baseline and follow-up AACs were 38 %. In 9 % of the cases one baseline AAC matched more than one follow-up AACs, and in 21 % of the cases the opposite occurred.

	Matches	Matches in pct.
Baseline	633	-
Follow-up	1222	-
Total match	240	38 %
Total one-to-many	57	9 %
Total many-to-one	134	21 %
Total no-match, baseline	255	40 %
Total no-match, follow-up	951	72 %

The mean size of the matched AACs was a little larger than the average baseline AAC - e.g. the mean height of all and the matched baseline AACs were 5.07 mm and 6.11 mm, respectively ($P < 0.001$) as shown in Table 3.

The characteristics of the growth of the AACs are shown in Table 3 and in Table 5. Table 3 shows the mean and standard deviations for height, width, and area of all and the matched AACs and the mean growth from baseline to follow-up. Table 5 shows the measured movement factors. The values are based on signed values. The results indicated that the overall growth in area was 57 % ($P < 0.001$), and that the matched AACs grew longitudinally with a average growth of 2.50 mm ($\pm$ 4.88 mm, $P < 0.001$), representing an increase of 41 %. The average growth in the radial direction was 0.50 mm ($\pm$ 1.55 mm, $P < 0.001$), corresponding to 21 %.

The AACs grew longitudinally. The linear correlation coefficients for all and matched AACs for the height, width, and area are shown in Table 4. Intuitively, there was correlation between growth in area and growth in height and width. There was also correlation between growth in width and height indicating that AACs grew both longitudinally and radially.

The AACs grew downstream. The average movement in the centre of masses was 0.60 mm ($\pm$ 2.69 mm,

Table 3 The growth patterns of the AACs. Note that the matched AACs were a little larger than the average baseline AACs, and that the AACs grew in all directions. The width, height, and area of the matched AACs were compared to the growth patterns of all AACs on a paired T-test. The baseline height-width ratio was compared to the follow-up height-width ratio on a paired T-test. The growth were tested with an un-paired T-test. *: P-value < 0.05, **: P-value < 0.01 and ***: P-value < 0.001.

	All Baseline	All Follow-up	Matched Baseline	Matched Follow-up	Growth in pct
Width (mm)	2.25 (±1.29)	2.30 (±1.67)	2.37 (±1.33)	2.87 (±1.61)***	21 % (±22 %)***
Height (mm)	5.07 (±3.84)	6.13 (±6.76)	6.11 (±3.95)***	8.61 (±5.34)***	41 % (±35 %)***
Area (mm^2)	171 (±200)	203 (±300)	211 (±224)*	329 (±329)***	57 % (±47 %)***
Height-Width ratio (mm)	2.33 (±1.38)	2.74 (±1.79)***	2.69 (±1.38)	3.38 (±1.02)***	20 % (±34 %)***

$P < 0.001$) in the longitudinal direction, as shown in Table 5. There was no evidence of the radial growth direction. The upper boundary of the AACs was moved 0.59 mm (± 3.55 mm, $P = 0.0116$) upwards the aorta, and the lower boundary was moved 1.85 mm (± 3.69 mm, $P < 0.001$) downward the aorta indicating the AACs mainly grew in the direction of the blood flow. The lumbar curvature and the inter-disk space did not change significantly over the study period.

4 Discussion

Important clinical insight of how atherosclerosis is progression could be found based on non-invasive longitudinal in vivo assessment of changes in the growth patterns of abdominal atherosclerotic calcified deposits from X-ray images. Examining the growth patterns of AACs from a large population (n > 100) is a new approach towards measurements of changes in the individual calcified deposits and could be a new marker of disease progression. Asymmetries in the growth of individual AACs suggests differences in the microscopic environments close to existing AACs.

Table 4 The linear correlation coefficient for all and matched AACs. All P-values < 0.001.

Correlation coefficient	Width vs. Height	Width vs. Area	Height vs. Area
Baseline (all)	0.5397	0.7812	0.8598
Follow-up (all)	0.6355	0.7405	0.7576
Baseline (matched)	0.4622	0.7881	0.8189
Follow-up (matched)	0.4265	0.7571	0.7759
Growth	0.4757	0.7636	0.7677

Table 5 The table shows the movement in the centre of mass and the upper and lower boundary of the AACs. Observe the AACs grew downstream the aorta.*: P-value < 0.05, **: P-value < 0.01 and ***: P-value < 0.001.

	Movement
ΔCY (mm)	0.60 (±2.69)***
ΔCX - posterior side, n=161 (mm)	0.03 (±0.98)
ΔCX - anterior side, n=73 (mm)	0.10 (±0.96)
ΔLower boundary (mm)	1.85 (±3.69)***
ΔUpper boundary (mm)	-0.59 (±3.55)**

The number of AACs increased. As shown in Figure 5, the subjects generally gained more calcified plaque mass over time. Both the number of AACs and the size of the existing baseline AACs increased, which indicate the possibility to derive new information about disease progression based on the growth of the existing AACs.

Subject-specific models of the disease progression. At present, the standard clinical practice is based on quantifying the severity of atherosclerosis, calculating the amount of calcified plaques, determining the narrowing of the aortic luminal, or calculating the intima-media thickness using X-ray, US, CT, or IVUS [25,6,26,22,23,27,17,16]. We believe that assessment of the growth potential of individual plaques could provide us with more understanding of the disease development, and this could lead to better tools for future risk assessment in patients suffering from atherosclerosis. Our evaluation of individual AACs may provide a new way of making subject-specific models of the progression of atherosclerosis. Future work will be on verifying our method in large scale longitudinal studies with different populations and refining of the growth patterns, but our results indicate the ability to measure changes in the individual AACs from X-ray images.

Longitudinal study. The detailed study of growth patterns of calcified deposits assessed over time is associated with certain challenges. It requires the ability to access the data at several time instances for the same subjects. This requirement was fulfilled with X-ray images. There exists several osteoporosis screening programs where X-ray images are collected at different time instances in a large patient cohort [15,28]. These programs could potentially be used for advancing the growth analysis. Likewise, there exists numerous longitudinal studies of how carotid atherosclerosis can predict myocardial infarction based on US imaging [16,17,29]. These US images could, possibly, also be used to derive growth patterns of the individual AACs, but in

the current study we have focused on the X-ray images. Previously conducted studies from CT and X-rays have focused on growth models based on arterial geometry, blood rate, and kinematics of finite growth combined with open system thermodynamics [30,31,11,4,10,32,33]. These studies have been based on cross-sectional data or a simulation model with a relative small population size (n<10). Our study is based on longitudinal data in order to increase the knowledge of the growth patterns. To our knowledge, this is the first study on a large population (n > 100) that investigates the longitudinal growth of the individual calcified deposits based on X-rays projections. We have analysed the predictive power of our model in respect to the known pathophysiology of atherosclerosis. The X-ray image modality has the advantages of a fast examination time, a low radiation exposure, a low cost, and non-invasiveness. These advantages of the X-ray image modality makes it possible to incorporate the growth patterns in large scale clinical studies and in population screening programs. X-rays have extensively been used to measure the quantity of the calcified plaques, but X-ray images could also play a qualitative role in risk assessment.
A limitation of X-ray images is the two-dimensional projection of the original three dimensional data. AACs are shown in the X-ray images due to a high attenuation. The high attenuation implies that the denser AACs on the anterior and posterior aorta wall are more easily detectable by the human eye compared to the AACs in the middle of the aorta. This means that the main part of the AACs in our study was aligned with the anterior or posterior aorta walls due to the manual annotations. Validation studies in which the two-dimensional shape and growth patterns are verified by using a three-dimensional image modality as well as an assessment of the observer variability are necessary to establish the final role of the validity of a growth pattern analysis.

Mainly AACs on posterior aorta wall. Figure 6 shows a probability map of the AACs at baseline and follow-up, respectively. The AACs were mainly formed in the lower part of the posterior aorta wall at baseline. At follow-up the number of AACs on the posterior aorta wall increased, but also new AACs on the anterior wall appeared. It has been shown that AACs are formed first in the lower lumbar regions and then progress to the upper lumbar regions [22,34]. This corresponds to our findings. Low flow velocity and recirculation zones at the posterior aorta wall could account for the increased number of posterior AACs [35]. The relative large number of AACs at the posterior aorta wall could also be caused by the use of manual annotations. In the areas close to the vertebrae, corresponding to the posterior aorta wall, it could be easier to confirm AACs while other anatomical structures can influence the judgement of AACs at the anterior aorta wall.

Suitable matching method. We have used a simple area overlap criterion for matching of AACs. Ongoing research has not yet clarified how the AACs emerge, coalesce, rupture, or get reabsorbed [4,36]. Due to the lack of knowledge about the behaviour of the growth of the AACs complicated matching routines with prior information about splitting, merging, creation, or disappearance of AACs are likely not able to increase the quality of the matching without biasing towards specific growth patterns at follow-up.
The matched baseline AACs were a little larger than the average baseline AACs. This was likely due to difficulties in matching the smaller registered AACs and the possibly increased activity in the growth of the new small AACs [37]. The size of all the AACs compared to the matched follow-up AACs also differed. New AACs were formed from baseline to follow-up resulting in a lower average size of all the AACs.
In an inter-observer study of the manual annotations, the radiologists had an area overlap of 50 %, and in an intra-observer study the area overlap was 60 %. The relatively low reproducibility in the manual annotations could account for a large number of the non-matched AACs. This could be refined by using automatic detection of AACs [38]. Misalignment in the registration could also account for some of the unmatched AACs. Further studies may improve the matching rate by a more advanced matching process and by using automated segmented AACs.

The AACs grew longitudinally. The AACs grew both longitudinally and radially. The calcified atherosclerotic plaque is at least four to five times more stiff than the soft plaque [4], and when the AACs occupy more of the aorta wall as they grow they are possibly making the aorta wall more stiff. The height-width ratio showed that the AACs grew more in height than in width. This could probably cause vascular stiffening and hypertension. The AACs are only a small part of the atherosclerotic plaques, so the overall growth in the plaque size is greater than what we have observed based on the growth patterns. The most valuable prognostic parameter would be the total surface area of the plaques rather than just the AACs, but X-ray projections are only able to visualise the calcified part of the plaques.

Downstream growth. The AACs grew downward the aorta, which could be caused by the turbulence in the direction of the blood flow where the aorta wall becomes non-smooth due to the existing AACs, as illustrated in Figure 7. This is in agreement with the clinical observation that plaques generally grow in the

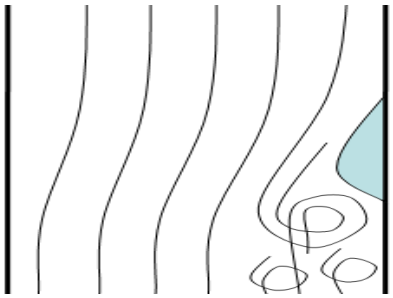

Fig. 7 An illustration of turbulence in the blood flow below an existing AACs. This could be a reason for the downstream growth of the AACs.

downstream direction [39, 40]. The turbulent flow fluid dynamics directly contribute to vascular damage and the initial plaque growth [41] and also contributes to the growth of the existing plaques. The downstream growth could also be an indication of different microscopic environments above and beneath the AACs.

Risk factors favours new AACs. The growth patterns were compared to the metabolic risk factors with Pearson's linear correlation coefficient and Kendall's tau, but no significant correlations showed up ($P < 0.05$). This could indicate that metabolic risk factors, like blood cholesterol, play a larger role in the initiation of the formation of AACs [37] but do not contribute much to the growth of the existing AACs. In [37] it is shown that the increase in severity morphological atherosclerotic calcification distribution (MACD) index is highly associated with the biochemical parameters, such as LDL cholesterol. In addition, the MACD index favours smaller plaques due to their large potential to growth and to the fact that risk of rupture decreases after the calcified phase of the plaques [4]. In our growth study, we have focused on existing AACs of a certain size due our to matching criterion. The pathology influencing the growth of these AACs could differ from the new smaller AACs. The growth of the existing AACs could be associated with local metabolic environmental changes, which are hard to capture at the macroscopic level. The asymmetries in the growth patterns for the different subjects indicate the need for large scale population to investigate the details of the progression of atherosclerosis, but it also indicates the possibility of deriving a per-subject based quantification of disease progression based on the growth patterns of AACs.

Acknowledgements We gratefully acknowledge the funding from the Danish Research Foundation (Den Danske Forskningsfond) supporting this work and the radiologists Paola C. Pettersen, Qing He, and Jianghong Chen from CCBR for providing the annotated X-rays used in this study.

References

1. Wilson, P.W.F., Kauppila, L.I., O'Donnell, C.J., Kiel, D.P., Hannan, M., Polak, J.M., Cupples, L.A.: Abdominal aortic calcific deposits are an important predictor of vascular morbidity and mortality. Circulation **103**, 1529–1534 (2001)
2. EHN: European heart network - european cardiovascular disease statistics 2008. `http://www.ehnheart.org/content/` (2008)
3. AHA: American heart association. `http://www.americanheart.org` (2009)
4. Abedin, M., Tintut, Y., Demer, L.L.: Vascular calcifications: Mechanisms and clinical ramifications. Arterioscler Thromb Vasc Biol. **24**, 1161–1170 (2004)
5. Eggen, D., Strong, J., McGill, H.: Calcification in the abdominal aorta: Relationship to race, sex and coronary atherosclerosis. Arch. of Path. **78**, 575–583 (1964)
6. de Weert, T.T., de Mony, C., Maijering, E., Booij, R., Niessen, W.J., Dippel, D.W.J., can der Lugt, A.: Assesment of atherosclerotic carotid plaque volume with multidector computed tomography angiography. Int J Cardiovasc Imaging **24**, 751–759 (2008)
7. Naghavi, M., Libby, P., Falk, E., Casscells, S.W., et al., S.L.: From vulnerable plaque to vulnerable patient: a call for new definitions and risk assessment strategies. Circulation **108**, 1664–1672 (2003)
8. Nissen, S.E., Yock, P.: Intravascular ultrasound novel pathophysiological insights and current clinical applications. Circulation **103** (2001)
9. Jin, H., Ham, K., Chan, J.Y., Butler, L.G., Kurtz, R.L., Thiam, S., Robinson, J.W., Agbaria, R.A., Warner, I.M., Tracy, R.E.: High resolution three-dimensional visualization and characterization of coronary atherosclerosis *in vitro* by synchrotron radiation x-ray microtomography and highly localized x-ray diffraction. Phys. Med. Bio. **47**, 1–12 (2002)
10. Kuhl, E., Maas, R., Himpel, G., Menzel, A.: Computational modeling of arterial wall growth. Biomech. Model **6**(5), 321–331 (2007)
11. Kaazempur-Mofrad, M.R., Younis, H.F., Isasi, A.G., Chan, R.R., Hinton, D.P., Sukhovam, G., LaMuraglia, G.M., Lee, R.T., Kamm, R.D.: Characterization of the atherosclerotic carotid bifurcation using mri, finite element modeling and histology. Ann. Biomed. Eng. **32**(7), 936–946 (2004)
12. Jacoby, D.S., Mohler, E.R., Rader, D.J.: Noninvasive atherosclerosis imaging for predicting cardiovascular events and assessing therapeutic interventions. Current Atherosclerosis Reports **6**(1), 20–26 (2004)
13. Kawasaki, M., Takatsu, H., Noda, T., Ito, Y., Kunishima, A., Arai, M., Nishigaki, K., Takemura, G., Morita, N., Minatoguchi, S., Fujiwara, H.: Noninvasive quantitative tissue characterization and two-dimensional color-coded map of human atherosclerotic lesions using ultrasound integrated backscatter: comparison between histology and integrated backscatter images. J. Am. Coll. Cardiol. **38**, 486–492 (2001)
14. Sodickson, A., Baeyens, P.F., Andriole, K.P., Prevedello, L.M., Nawfell, R.D., Hanson, R., Khorasani, R.: Recurrent ct, cumulative radiation exposure, and associated radiation-induced cancer risks from ct of adults. Radiology **251**, 175–184 (2009)
15. Tanko, L.B., Bagger, Y.Z., Gerong Qin, P.A., Larsen, P.J., Christiansen, C.: Enlarged waist combined with elevated triglycerides is a strong predictor of accelerated atherogenesis and related cardiovascular mortality in postmenopausal woman. Circulation **111**(15), 1883–1890 (2005)
16. Mallett, C., House, A.A., Spence, J.D., Fenster, A., Parraga, G.: Longitudinal ultrasound evaluation of carotid atherosclerosis in one, two and three dimensions. Ultasound in Med. and Biol. **35**(3), 367–375 (2009)

17. Patel, A.S., Mackey, R.H., Wildman, R.P., Thompson, T., Matthews, K., Kuller, L., Sutton-tyrell, K.: Cardiovascular risk factors associated with enlarged diameter of the abdominal aortic and iliac arteries in healthy women. Atherosclerosis **178**, 311–317 (2005)
18. Ahlgren, A.R., Hansen, F., Sonesson, B., Lanne, T.: Stiffness and diameter of the common carotid artery and abdominal aorta in women. Ultrasound in Med. and Biol. **23**(7), 983–988 (1997)
19. Brady, A.R., Thompson, S.G., Fowkes, F.G., Greenhalgh, R.M., Powell, J.T.: Abdominal aortic aneurysm expansion: risk factors and time intervals for surveillance. Circulation **110**, 16–21 (2004)
20. Chang, J.B., Stein, T.A., Liu, J.P., Dunn, M.E.: Risk factor associated with rapid growth of small abdominal aortic aneurysms. Surgery **121**(2), 117–122 (1997)
21. Lindholt, J., Heegaard, N., Vammen, S., Fasting, H., Henneberg, E., Heickendorff, L.: Smoking, but not lipids, lipoprotein (a) and antibodies against oxidised ldl, is correlated to the expansion of abdominal aortic aneurysms. European journal for Vascular Evdovascular Surgery **21**, 51–56 (2001)
22. Kauppila, L.I., Polak, J.F., Cupples, L.A., Hannan, M.T., Kiel, D.P., Wilson, P.W.F.: New indices to classify location, severity and progression of calcified lesions in the abdominal aorta: a 25-year follow-up study. Athero **132**, 245–250 (1997)
23. Kiel, D.P., Kauppila, L.I., Cupples, L.A., Hannan, M.T., ODonnell, C.J., Wilson, P.W.F.: Bone loss and the progression of abdominal aortic calcification over a 25 year period: The framingham heart study. Calc. Tis. Int. **68**, 271276 (2001)
24. Bookstein, F.L.: Principle warps: Thin-plate splines and the decomposition of deformation. IEEE Trans. pattern anal. machine int. **11**(6), 567–584 (1989)
25. Agatston, A.S., Janowitz, W.R., Hildner, F.J., Zusmer, N.R., Viamonte, M.J., Detrano, R.: Quantification of coronary artery calcium using ultra fast computed tomography. J. Amer. Col. Card. **15**, 827–832 (1990)
26. Ibanez, B., Pinero, A., Orejas, M., Badimon, J.J.: Novel imaging techniques for quantifying overall atherosclerotic burden. Rev. Esp. Card. **60**(3), 299–309 (2007)
27. Reiber, J.H., Koning, G., Dijkstra, J., Wahle, A., Goedhart, B., Sheehan, F.W., Sonka, M.: Handbook of Medical Imaging, vol. 2 - Medical Image Processing and Analysis, chap. Angiography and Intravascular Ultrasound. SPIE Press (2000)
28. Hannan, M.T., Felson, D.T., Dawson-Hughes, B., Tucker, K.L., Cupples, L.A., Wilson, P.W., Kiel, D.P.: Risk factors for longitudinal bone loss in elderly men and women: the framingham osteoporosis study. J. Bonr Miner. Res. **15**(4), 710–720 (2000)
29. Johnson, S.H., Matthiesen, E.B., Joakimsen, O., Stensland, E., Wilsgaard, T., Loechen, M.L., Njoelsland, I., Arnesen, E.: Carotid atherosclerosis is a stronger predictor of mycardial infarction in women than in men - a 6-year folloe-up study of 6226 persons: The troms study. Stroke **38**, 2873–2880 (2007)
30. Boyd, J., Buick, J.M., Cosgrove, J.A., Stansell, P.: Application of the lattice boltzmann model to simulated stenosis growth in in the two-dimensional carotid artery. Phy. Med. Bio. **50**, 4783 – 4796 (2005)
31. Chatziprodromou, I., Poulikakos, D., Ventikos, Y.: On the influence of variation in haemodynamic conditions on the generation and the growth of cerebral aneurysms and the atherogenesis: A computational model. J. Biomech. **40**, 3626–3640 (2007)
32. Taylor, C.A., Hughes, T.J.R., Zarins, C.K.: Finite element modeling of the three-dimensional pulsatile flow in the abdominal aorta: Relevance to atherosclerosis. Ann. Biomed. Eng. **50**, 975–987 (1998)
33. Zohdi, T.I., Holzapfel, G.A., Berger, S.A.: A phenomenological model for atherosclerotic plague growth and rupture. J. Theo. bio. **227**, 2437–2443 (2004)
34. Witteman, J.C.M., Kok, F.J., Saase, J.L.C.V., Valkenburg, H.A.: Aortic calcifications as a predictor of cardiovascular mortality. Lancet **2**, 1120–1122 (1986)
35. Tang, B.T., Cheng, C.P., Draney, M.T., Wilson, N.M., Tsao, P.S., Herfkens, R.J., Taylor, C.A.: Abdominal aortic hemodynamics in young healthy adults at rest and during lower limb exercise: quantification using image-based computer modeling. Amer. J. Phys: Heart and circ. Phys. **291**(2), 668–676 (2006)
36. Farzaneh-Far, A., Proudfoot, D., Shanahan, C., Weissberg, P.L.: Vascular and valvar calcification: Recent advances. Heart **85**, 13–17 (2001)
37. Barascuk, N., Ganz, M., Nielsen, M., Register, T.C., Rasmussen, L.M., Karsdal, M.A., Christiansen, C.: Abdominal aortic calcification quantified by the morphological atherosclerotic calcification distribution (macd) index is associated with features of the metabolic syndrome (2009). In review
38. Lauze, F., de Bruijne, M.: Toward automated detection and segmentation of aortic calcifications from radiographs. Medical Imaging, Proceedings of SPIE (2007)
39. Olgac, U., Kurtcuoglu, V., Saur, S.C., Poulikakos, D.: Identification of atherosclerotic lesion-prone sites through patient-specific simulation of low-density lipoprotein accumulation. In: MICCAI, vol. 2, pp. 774–781 (2008)
40. Smedby, O.: Do plaques grow upstream or downstream? an angiographic study in the femoral artery. Atherosclerosis, Thrombosis, and Vascular Biology **17**(5), 912–918 (1997)
41. Conrad-Hansen, L.: Phd dissertation: Towards an automated quantification tool for the assessment of atherosclerotic plaque in lumbar x-rays. Ph.D. thesis, Department for Computer Science, University of Copenhagen (2007)